Revista Brasileira de Cartografia (2013) N⁰ 65/4: 747-755
Sociedade Brasileira de Cartografia, Geodésia, Fotogrametria e Sensoriamento Remoto
ISSN: 1808-0936

RELATIONSHIPS BETWEEN REMOTELY SENSED FOREST STRUCTURE AND BIOMASS: FOURIER STRUCTURE FROM LIDAR AND INSAR AND PENETRATION AT MICROWAVE FREQUENCIES

Relação entre Biomassa e Dados Sensoriados de Estrutura Florestal: Estrutura Fourier Derivada por LiDAR e InSAR e Penetração em Freqüências de Microondas

Robert Treuhaft[1]; Fabio Guimarães Gonçalves[2]; Bruce Chapman[1]; Maxim Neumann[1]; João Roberto dos Santos[3] & Paulo Maurício Lima de Alencastro Graça[4]

[1]National Aeronautics and Space Administration – NASA
Jet Propulsion Laboratory, California Institute of Technology
4800 Oak Grove Drive, 138-212, Pasadena, CA 91109 - USA
{robert.treuhaft, bruce.d.chapman, maxim.neumann}@jpl.nasa.gov

[2]The Woods Hole Research Center
149 Woods Hole Road, MA 02540 - USA
fgoncalves@whrc.org

[3]Instituto Nacional de Pesquisas Espaciais – INPE
Divisão de Sensoriamento Remoto – DSR
Av. dos Astronautas, 1758, 12.227-010 – São José dos Campos - Brasil
jroberto@dsr.inpe.br

[4]Instituto Nacional de Pesquisas da Amazônia – INPA
Av. André Araújo, 2936, 69083-000, Manaus, AM-Brasil,
pmlag@inpa.gov.br

Recebido em 06 de dezembro, 2012/ Aceito em 25 de janeiro, 2013
Received on December 06, 2012/ Accepted on January 25, 2013

ABSTRACT

This paper proposes the correlation of biomass with Fourier transforms of LiDAR and InSAR vegetation density measurements at vertical and horizontal Fourier spatial frequencies, as a means to estimate biomass. It further suggests that each Fourier frequency of leaf area density could be modeled as a harmonic oscillator, in which leaf area itself provides a restoring force to constrain it to some nominal value. Preferred Fourier frequencies for tropical forest stands at La Selva Biological Station, Costa Rica, with vertical wavelengths of 12 to 18 m and 5-7m are shown from LIDAR as an

update to previous work. These two wavelengths are close to the average height and crown depth of forest stands measured. As an example of different kinds of modeling, it is suggested that biomass be considered a complex quantity with amplitude representing the usual biomass, and the phase representing some undetermined characteristic of the forest. Finally, since structure-based biomass estimation will presumably improve with signal penetration, a diffraction calculation of penetration through holes at L- and C-band shows that the diffractive component of penetration from C-band is greater than or equal to that at L-band, countering to some extent the lower penetration at C-band due to the frequency dependence of water's extinction.

Keywords: Forest Structure, InSAR, LiDAR, Biomass, Tropical Forest, Forest Inventory, Monitoring.

RESUMO

Esse trabalho propõe o uso da correlação entre biomassa e transformadas de Fourier de perfis de densidade de vegetação obtidos por LiDAR ou InSAR em várias frequências espaciais, tanto verticais como horizontais, como um meio de se estimar biomassa em florestas tropicais. Sugere ainda que cada frequência de Fourier de densidade de área foliar poderia ser modelada como um oscilador harmônico, onde a área foliar é usada para se restringir a força restauradora a algum valor nominal. Frequências de Fourier preferenciais de florestas tropicais na Estação Ecológica La Selva, Costa Rica, com comprimentos de onda vertical de 12 e 18 m e 5-7 m, são apresentadas de LIDAR como uma atualização de trabalho anterior. Esses dois comprimentos de onda são próximos ao da altura média e da profundidade de copa das florestas mensuradas. Como um exemplo de diferentes abordagens de modelagem, sugere-se que a biomassa seja considerada como uma quantidade complexa, com a amplitude representando a biomassa usual e a fase representando alguma característica sub-determinada da floresta. Por fim, conduziu-se um cálculo de penetração através de aberturas no dossel, com bandas L e C, com o intuito de avaliar a presunção de que a estimativa de biomassa a partir de dados de estrutura melhora com uma maior penetração do sinal. Os resultados mostram que o componente de difração de penetração em banda C é maior ou igual àquele em banda L, contrariando o conceito comumente difundido de menor penetração em banda C devido à maior extinção da radiação promovida pelo conteúdo de água na vegetação.

Palavras-chave: Estrutura Florestal, InSAR, LiDAR, Biomassa, Floresta Tropical, Inventário, Monitoramento.

1. INTRODUCTION

It is widely accepted that the structure of forests is highly correlated with aboveground biomass, and that LiDAR (LEFSKY *et* al. 2002) and interferometric Synthetic Aperture Radar (InSAR) (TREUHAFT *et al*. 2004) are the principal optical and microwave remote sensing techniques to estimate that structure. There is a wide variation in the structural variables that have been used for biomass estimation, including vegetation median or total tree height (DRAKE *et al*. 2002, LiDAR; NEEFF *et al*. 2005a, InSAR), standard deviation (TREUHAFT *et al*. 2003, InSAR), quadratic mean height (NELSON *et* al. 2007, LiDAR), and fractional canopy heights (LEFSKY 2010, LiDAR). There are also approaches which estimate diameter distributions from radar power and height, which can potentially be applied to biomass estimation (NEEFF *et al*. 2003). There is no agreed-upon set of structural descriptors that is universally used, even within the same type of forest.

This paper elaborates the arguments in TREUHAFT *et al*. (2010) for using the Fourier transform of vertical vegetation distributions at various spatial frequencies to estimate aboveground biomass. It starts by discussing the general biomass-estimation problem, how structure might relate to biomass, and the Fourier transform, in both vertical and lateral directions, as a general means to characterizing mechanism-driven spatial variability of vegetation density. It then shows biomass estimation results using Fourier transforms of LiDAR waveforms, updating TREUHAFT *et al*. (2010), and discusses alternative possibilities for modeling biomass as a function of structure.

Because biomass is expressed as a function of the complex components of the Fourier transform, this paper also considers the natural extension of casting biomass itself as a complex quantity, with amplitude and phase of SAR data. Finally, the question of penetration - of how signals at C- and L-band see through the holes or gaps in the forest - is preliminarily addressed, because the efficacy of remotely sensed structure depends on microwave signal penetration.

2.BIOMASS ESTIMATION FROM STRUCTURE AND THE 1-D AND 3-D FOURIER TRANSFORM

If trees are considered to be cylinders, or tapered cylinders, and the graduated diameter as a function of vertical distance above the ground were known, along with the wood density as a function of vertical distance, the mass of each tree trunk, about 75% of the total tree mass (SCHELSINGER, 1991), could be calculated. If the mass of branches, twigs and leaves could similarly be measured, the total mass of the tree would, in principle, be known. Typical field work measurements including the more restricted data set of diameter at breast height (DBH) and total height are usually used, along with wood density from species identification, yielding typical errors of about 10% (CHAVE *et al*., 2004; CHAVE *et al*., 2005). The field-measured biomass (meaning "biomass area density" in Mg/ha) would then have similar accuracy. For remote sensing, the situation is different. There is no remote sensing technique, suitable for spaceborne, regional or global acquisition, which can uniquely measure DBH, wood density, and height at the tree level.

The challenge for the practice of biomass estimation from remotely sensed structure is: To what aspects of that structure is biomass at 0.25-1 ha scales most sensitive? The lateral spatial scales mentioned are typical of remote sensing data and scales over which change takes place. We will assume here, as is often done, that the profiles measured by InSAR or LiDAR are closely related to leaf area density - LAD (TREUHAFT *et al*. 2003; TREUHAFT *et al*. 2009).

The Fourier transform of the vertical profile of radar power $\gamma(f)$, at frequency *f*, might begin to point to biophysical mechanisms by which canopies are organized, as suggested below. This vertical transform can be extracted from the InSAR cross correlation at a given baseline (TREUHAFT *et al*. 1996) as

$$\gamma(f) = \frac{\int_0^\infty g(z)\,\exp[i2\pi fz]\,dz}{\int_0^\infty g(z)\,dz} \qquad (1)$$

where *f* is a function is of baseline length and other geometric parameters, and the wavelength. In (1), g(z) is the radar power profile, assumed to depend on the leaf area density (LAD) profile and attenuation characteristics, the latter of which are generally taken to be more severe at higher microwave frequencies.

An expression similar to (1) can be derived for the Fourier transform of LiDAR with g(z) replaced by the LiDAR waveform (TREUHAFT *et al*. 2010). For either the LiDAR or the InSAR Fourier transform, g(z) has been found to be very close to the LAD, i.e. attenuation does not seem to change the power profile very much in some studies (e.g. TREUHAFT et al. 2009). Below, therefore, g(z) will be referred to as the "LAD profile," but in general some transformation between the radar power profile (TREUHAFT et al. 1996) or the LiDAR profile (MACARTHUR and HORN 1969) and the LAD profile may be necessary.

The Fourier transform is the natural result of InSAR at a given baseline and an easily calculated result from LiDAR. It can be seen with the inverse Fourier transform in (2), used in tomography, that the Fourier transform can be thought of as the amount of the vertical profile oscillating at vertical spatial frequency *f*:

$$\frac{g(z)}{\int_0^\infty g(z)\,dz} = \frac{1}{2\pi}\int_{-\infty}^{\infty}\gamma(f)\,\exp[-i2\pi fz]\,d(2\pi f) \equiv \int_{-\infty}^{\infty} g_f(z)\,df \qquad (2)$$

where $g_f(z)$ is defined by (2) and is the strength of the part of the normalized LAD profile which oscillates at frequency *f* in the vertical direction.

Performing regression of forest biomass to the Fourier transform at a small number of frequencies, *f*, can potentially identify which of these Fourier frequency components of the LAD profile most affect biomass. Each Fourier component $g_f(z)$, harmonically oscillating at *f*, can be thought of as arising from a differential equation of the form

$$\frac{d^2 g_f(z)}{dz^2} = -(2\pi f)^2 g_f(z) \qquad (3)$$

This differential equation in (3) is that of a spring's displacement, where that displacement is replaced by the vegetation density, and time is replaced by the vertical coordinate *z*. The restoring force on the right side of (3) is proportional to the square of the frequency and to the vegetation density at *z* itself. For a forest vertical profile, (3) suggests

that there is some mechanism restoring the vertical density to a mean value - the value at $f = 0$. If, at a given point z, the density substantially exceeds that mean value, the second derivative of density as a function of z – the right side of (3) – points toward reducing the derivative of density with respect to altitude. One could imagine patterns of shade or features of tree physiology acting to restore LAD to a mean value.

Such a pattern is schematically depicted in Figure 1. In this Figure, the electric field from the sun's light is incident along the direction of the arrow, with plane waves indicated by the parallel black lines on the left. The canopy of the small tree constitutes one vertical enhancement of LAD - indicated by the lower green ova - and, at the same time, it shades the tall tree, preventing LAD from accruing on its lower trunk. The tall tree then presents a vertical enhancement of LAD at higher altitudes only. The two enhancements from the mechanism on the left of Figure 1 create the aggregate profile on the right, with characteristic vertical period given by the distance between peaks of the red curve. That profile could be remotely sensed by either LiDAR or InSAR as a Fourier component with a vertical frequency corresponding to that period.

A biomass correlation with preferred frequencies might suggest dynamical models describing the restoring force, perhaps based on resource competition as in Figure 1. Dynamical models might account for this restoring force preventing leaf area from moving too far away from its mean value, and for the nature of the correlation between the restoring force and the biomass value.

The potential connection with dynamical models which isolate vertical restoring mechanisms, or other mechanisms determined by sets of preferred Fourier frequencies and alternatives to (3), is a key argument for decomposing profiles into Fourier components via (1).

A natural extension of the vertical Fourier transform of (1) is the 3-D transform:

$$\gamma_{3\_D}(f_x, f_y, f_z) = \frac{\int_0^\infty g(x,y,z)\, e^{j2\pi f_z z} e^{j2\pi f_x x}\, e^{j2\pi f_y y}\, dz\, dx\, dy}{\int_0^\infty g(x,y,z)\, dz\, dx\, dy} \quad (4)$$

where g(x,y,z) is now a 3-D LAD, or radar power or LiDAR density. Biomass on a 0.25-1 ha plot could similarly be imagined to be sensitive to $\gamma_{3\text{-}D}$ for some lateral and vertical frequencies f_x, f_y, f_z. Lateral sensitivity of biomass has been found, for example, by ECKERT (2012) and a correspondence of X-band power and lateral distribution has been found by NEEFF *et al*. (2005b). Using (4) might lead to similar physical mechanisms regarding restoring the vegetation density to a mean value in the lateral direction at frequencies f_x and f_y. If

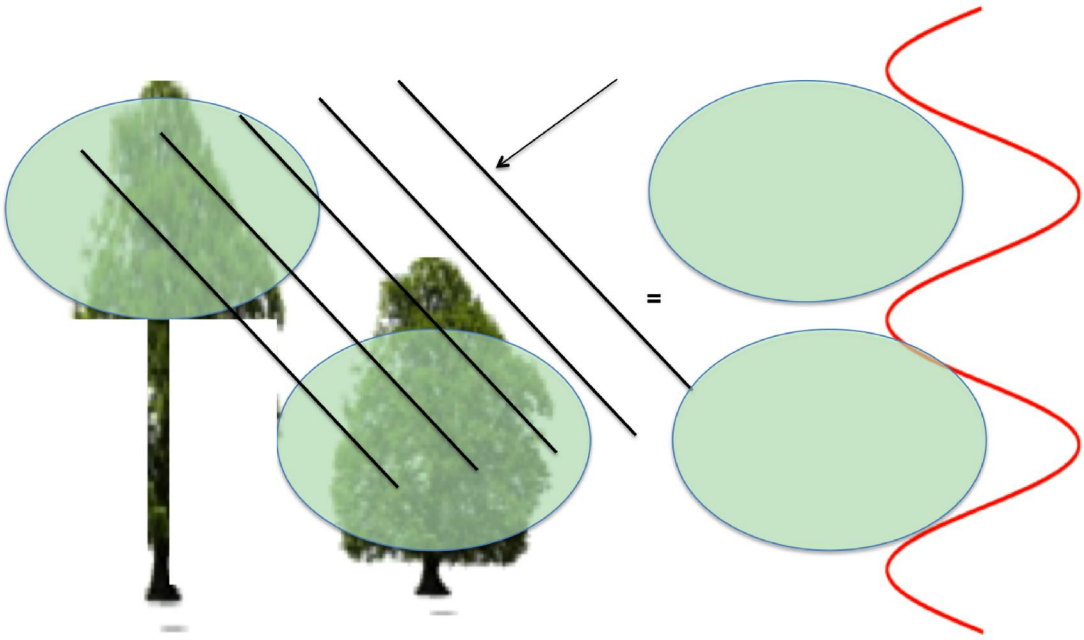

Fig. 1 - Schematic diagram of how a pattern of shading might create a Fourier component described by (3). The short tree shades the taller one, creating an oscillating pattern of LAD as a function of height, as indicated by the red curve.

biomass is correlated with those frequencies, it might lead to biophysical explanations as to why it should correlate with restoring forces on different spatial scales. The 3-D density function g(x,y,z) could be realized by small-spot LiDAR profiles measured at many lateral locations within a 0.25-1 ha area. Since an InSAR baseline corresponds to the vertical frequency f_z, multiple horizontally sampled InSAR measurements with a few baselines could generate $\gamma_{3\text{-}D}(f_x,f_y,f_z)$. However, side-looking InSAR averages over lateral distances of the order of a tree height (see e.g. Figure 1 from TREUHAFT *et al*. 1996), no matter what the fundamental resolution of the radar is. Interpretations of (4) applied to small-spot LiDAR and InSAR will have to consider differences in results on the spatial scales over which InSAR is averaging.

Also note that topographic slopes will effectively couple horizontal and vertical distributions, if not calibrated and removed. This coupling may introduce relationships between the horizontal and vertical frequencies in (4). There may be biophysical relationships between horizontal and vertical distributions as well, as terrain slopes can change the vertical organization of the canopy due to induced changes in light penetration and crown exposure (BISPO *et al*. 2012).

3.PREFERRED FOURIER FREQUENCIES FOR BIOMASS ESTIMATION AND BIOMASS AS A COMPLEX QUANTITY

As described in TREUHAFT *et al*. (2010), a general approach to selecting InSAR baselines for forest structure and biomass monitoring might be to use Fourier transforms of LiDAR data and determine InSAR baselines corresponding to the LiDAR Fourier frequencies producing the best biomass estimates. This approach assumes that profiles from LiDAR and InSAR are similar, as they were qualitatively in TREUHAFT *et al*. (2009) for C-band (wavelength = 0.056 m) InSAR. But this approach must be verified with more experiments at C-band and other radio frequencies, especially L-band (wavelength = 0.24 m). At La Selva Biological Station in Costa Rica, 27 tropical rainforest stands 50 m x 50 m were measured with 14 baselines of AirSAR InSAR in 2004 (VAN ZYL *et al.* 1997) and LVIS LiDAR in 2005 (BLAIR *et al*. 2006). Of the 27 plots, 18 were primary forests, with 6 selectively logged among them, 6 were secondary forests, and 3 were abandoned pastures. Field measurements were done at La Selva in 2006, on 10 m x 100 m transects, consisting of diameter at breast height, tree position, total height, height-to-base-of-crown, and canopy dimensions (TREUHAFT *et al.* 2009). Biomass for each stand was estimated by allometric equations from field data using an average wood density which scaled linearly with diameter class (CHAVE *et al*. 2004, TREUHAFT *et al.* 2010).

Figure 2 shows the RMS scatter of the field biomass about model biomass, taken as

$$B_{\text{model}} = a + b_{real}\, real\ part(\gamma(f)) + b_{imag}\, imag\ part(\gamma(f)) + b^{1st}_{real}\, real\ part(\gamma'(f)) + b^{1st}_{imag}\, imag\ part(\gamma'(f)) + b^{2nd}_{real}\, real\ part(\gamma''(f)) + b^{2nd}_{imag}\, imag\ part(\gamma''(f)) \quad (5)$$

where the Fourier transform g(f) comes from LVIS LiDAR data using (1), g'(f) is the first derivative of the Fourier transform with respect to frequency, and g''(f) is the second derivative. It was found that (5) with the derivatives performs as well as (6) in TREUHAFT et al. (2010). The real a and b coefficients in (5) were estimated by minimizing the RMS difference, on the y-axis in the Figure, between field-measured biomass and Bmodel for the 27 stands.

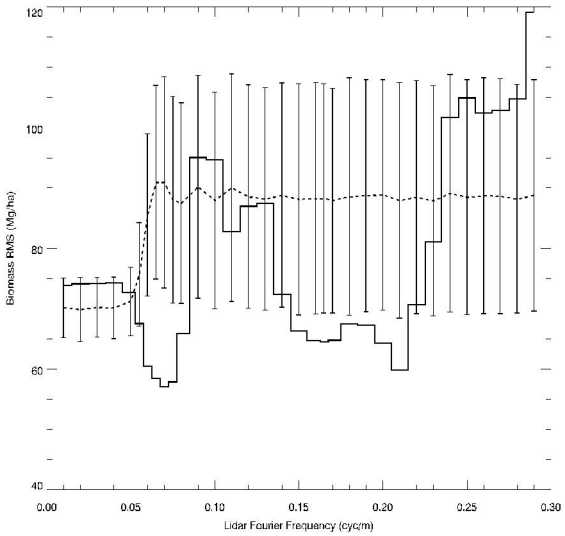

Fig. 2 - The RMS scatter of field biomass about model biomass as a function of frequency *f* as in (5) for 27 forest stands observed with LVIS LiDAR at La Selva. The dashed line and error bars result from a simulation in which, aside from height, there is no dynamical correlation of profile characteristics with biomass.

In Figure 2, the dashed line is the average scatter from a simulation in which there was no correlation of biomass with structure beyond average height (Fourier $f = 0$). The error bars show the standard deviation of the scatter in the absence of any real correlation with Fourier frequencies greater than zero. The RMS using height only is about 76 Mg/ha, using height and standard deviation, about 72 Mg/ha. The solid black line, the RMS of field biomass about model biomass, has to substantially miss the error bars to indicate a significant improvement over height-based estimation by using Fourier transforms. This happens between 0.055 and 0.08 cyc/m, or for characteristic vertical scales of 12 to 18 m. If X-band and LiDAR profiles were similar, these optimal Fourier frequencies would correspond to a baseline of about 780 m for TanDEM-X (KRIEGER *et al*. 2010). There is also an indication of performance improvement at 0.15-0.21 cyc/m, corresponding to vertical wavelengths of 5 - 7 m. These two preferred ranges of Fourier wavelength are closed to the field-measured average total height (~20 m) and crown depth (~7m), respectively. The height and crown depth averages are all trees measured in 27 plots at La Selva, spanning abandoned pastures, secondary and primary forest. The differences between Figure 2 here and Figure 3 of TREUHAFT *et al*. (2010) result almost entirely from an improved ground-detection algorithm used here, and removing one outlier which had a fairly steep slope of more than

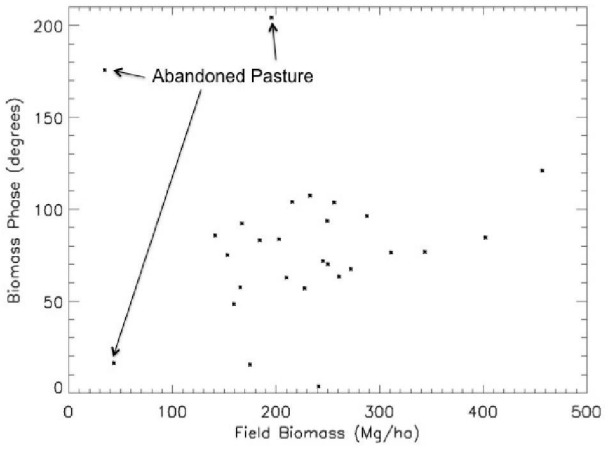

Fig. 3 - Biomass phase, when biomass at La Selva is modeled by a complex equation as in (6). The three abandoned (within 6 years of measurements) pasture stands are indicated with arrows. All other stands are primary, secondary, or selectively logged forest.

20 degrees. The improved algorithm uses LiDAR signal-to-noise thresholds to decide in which LiDAR bin the ground is first detected. Previously, the ground had been identified as the first peak beyond a nominal point established by eye. Figure 2 is only meant as a demonstration of how one might use LiDAR profiles to suggest optimal Fourier frequencies and InSAR baselines. The optimal Fourier frequencies found in the La Selva data may not at all reflect optimal frequencies in other data sets.

Because (5) casts biomass as a function of the complex parts of the Fourier transform, we also considered biomass itself to be a complex number, replacing (5) with:

$$B_{model} = a + b\,\gamma(f) + b^{1st}\,\gamma'(f) + b^{2nd}\,\gamma''(f) \quad (6)$$

where a, b^{1st} , and b^{2nd} are all complex, as is B_{model} on the left of (6). The complex parameters were determined for Figure 3 by requiring the RMS of the difference between field-measured biomass and the magnitude of B_{model} be as small as possible for the La Selva data. The Fourier frequency was 0.07 cyc/m and the RMS of the biomass amplitude was 57 Mg/ha, similar to when biomass is considered real.

Figure 3 shows the biomass phase, when the scatter of the amplitudes was minimized about field-measured biomass. The overall phase is arbitrary. Only stand-to-stand variations result from (6). As of this moment, there is no clear interpretation of the biomass phase, but it seems to grow from about 20 to 100 degrees over the range of biomasses measured. There is also the suggestion that the biomass phase of at least two of the three abandoned pastures, pointed out with arrows, may be different than those of other stands. The biomass phase should be studied more carefully to determine if it has substantial value for biomass estimation performance.

4. PENETRATION AT MICROWAVE FREQUENCIES

The efficacy of structure information from remote sensing in estimating biomass depends in part on the degree to which the microwave frequency of the radar penetrates forest vegetation. Recent results in tropical forests (TREUHAFT *et al*. 2009;

HAJNSEK *et al*. 2009) suggest that higher microwave frequencies (C-band and X-band) may be useful for estimating vegetation profiles and/or heights. In TREUHAFT *et al*. (2009), it is suggested that lateral gaps in the tropical forest observed from fieldwork may in part account for why C-band seems to penetrate, to see the entire vegetation profile. The premise explored here is that when lateral gaps in the forest are of the order of a few wavelengths and bigger, the wave will penetrate those gaps. Narrow gaps would then favor higher frequencies (shorter wavelengths), while the extinction of water as a function of frequency in the absence of gaps favors lower frequencies. Below is a calculation which, for simplicity, replaces the canopy with an opaque screen 10 m above the surface, with one square gap. The beam is transmitted at 35 degrees incidence. The point of this calculation is an illustration of the penetration into gaps at L- and C-band, without considering the frequently-cited increased attenuation at C-band relative to L-band (JACKSON 1975).

The geometry of the calculation is shown in Figure 4. The field, taken to be horizontally polarized into the plane of the paper, propagates from the radar at the upper left, and only penetrates the screen (canopy) at the hole. The field at the coordinate $\vec{x}'$ at the hole, $E(\vec{x}')$, and its derivatives in the direction of the normal $\hat{n}$ in the Figure are needed in the calculation. The diffracted field at a ground surface point, $\vec{x}_G$, shown at the origin in the Figure, due to a field transmitted at ,is (STRATTON and CHU 1939, TREUHAFT *et al*. 2011)

$$E(\vec{x}_G) = \frac{1}{4\pi}\int_S \left[E(\vec{x}')\vec{\nabla}G(\vec{x}_G,\vec{x}') - G(\vec{x}_G,\vec{x}')\vec{\nabla}E(\vec{x}') \right] \bullet \hat{n}\, d^2x'$$

$$G(\vec{x}_G,\vec{x}') \equiv \frac{e^{ik|\vec{x}_G-\vec{x}'|}}{|\vec{x}_G-\vec{x}'|} \quad and \quad E(\vec{x}') \propto \frac{e^{ik|\vec{x}'-\vec{x}_T|}}{|\vec{x}'-\vec{x}_T|} \tag{7}$$

where the field on the hole surface is shown in (7) to be a spherical wave with wavenumber $k = 2\pi/\lambda$, with λ the radar wavelength. The surface integral in (7) is along the underside of the opaque screen and in the hole, as indicated in Figure 4.

Using (7), Figure 5 shows the field strength seen by the ground as a function of distance in the plane of the paper in Figure 4 away from $\vec{x}_G = 0$. It can be seen that for 1-m holes — a few tens of

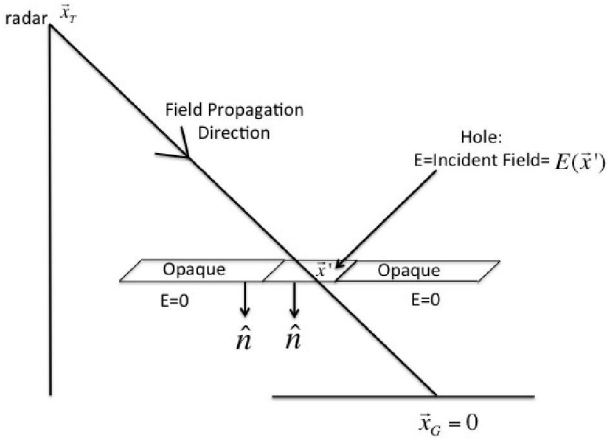

Fig. 4 - The geometry for the calculation of the field due to a canopy simulated by an opaque screen with a square hole. $\vec{x}_G$ is the location on the ground at which the field is calculated, shown at the origin in the Figure. $\vec{x}_T$ is the position of the transmitter, $\hat{n}$ is the surface normal, and $E(\vec{x}')$ is the field in the hole.

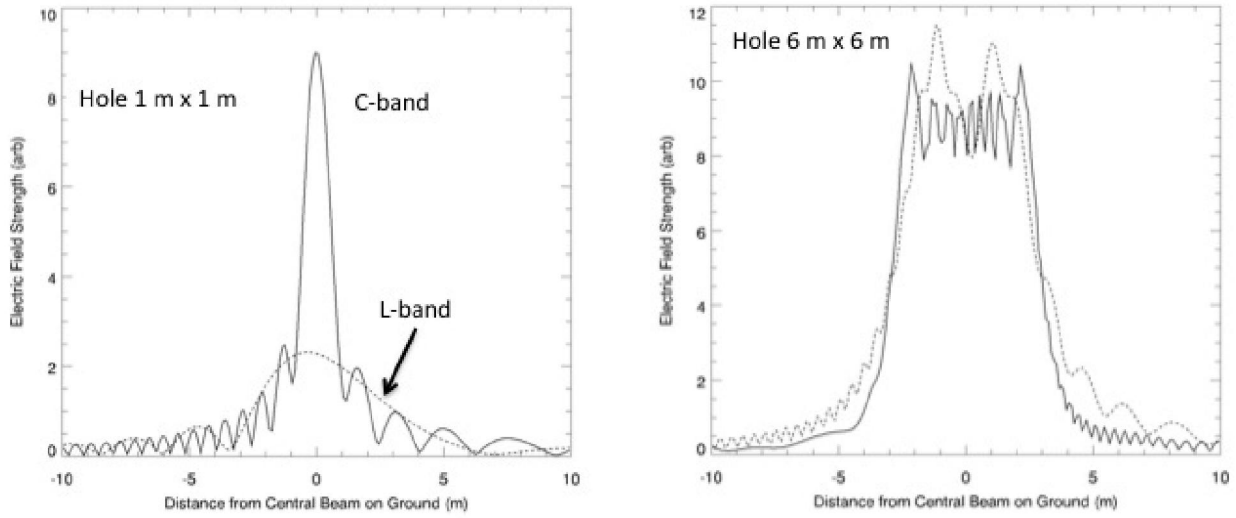

Fig. 5 – The calculated electric field strength at L- (dotted) and C-band (solid) as a function of distance from the central beam on the ground for a 1 m x 1 m square hole and one 6 m x 6 m, not considering the increased attenuation at C-band relative to L-band to water absorption.

wavelengths at C-band ($\lambda = 0.56$ m) and only about 4 wavelengths at L-band ($\lambda = 0.24$ m) — C-band penetration is greater than L-band, due to diffraction alone. When the hole is 6 m x 6 m, the effects of diffraction are similar for the two wavelengths. It must be remembered that the greater absorption of the wave at C-band will reduce C-band amplitudes relative to L-band. The point of Figure 5 is simply to say that an understanding of these competing mechanisms, quantitatively compared, may help to explain why higher frequencies sometimes seem to penetrate more than expected.

5. SUMMARY

This paper states the regression of biomass to vertical Fourier transforms of LiDAR and InSAR in (1), (2), and (5). It further suggests that a single Fourier component could result from a biophysical mechanism in which there is an effective restoring force (3), driving LAD to some equilibrium value. We suggest in Figure 1 that patterns of shade or features of tree physiology might act to keep LAD from straying too far from mean values, but the biophysical mechanisms should be considered with forest dynamical models. Figure 2 is an update of previous vertical Fourier biomass results from La Selva, using improved LiDAR ground-finding algorithms. Preferred vertical wavelengths of 12-18 m are more clearly identified for this La Selva data set, and there is some indication that wavelengths of 5-7 m also show improved performance in ongoing work. Other data sets may have other (or no) preferred Fourier frequencies, though ongoing work suggests similar optimal frequencies in Tapajós National Forest, Brazil. A 3-dimensional extension of the vertical Fourier transform for biomass regression is proposed in (4). A currently active project using TanDEM-X interferometric and small-spot LiDAR data at Tapajós should shed light on the potential of 3-D Fourier transforms for biomass estimation. Because biomass is being expressed in (5) as a function of real and imaginary parts of Fourier structure, we propose investigating a complex biomass, in which its magnitude is what we normally call 'biomass', and its phase may have some physical meaning as suggested by the biomass phase of Figure 3. Because 3-D characterization of forests will depend on penetration, and because higher frequencies frequently seem to penetrate more than expected, Figure 5 shows the results of a Kirchoff diffraction calculation, in which, by diffraction alone, C-band penetrates better through small holes than L-band. This effect, however, is countered by higher absorption of electromagnetic waves at C-band, due to the dielectric constant of water at microwave frequencies.

ACKLNOWLEDGMENT

The research described in this paper was carried out in part by the Jet Propulsion Laboratory, California Institute of Technology, under contract with the National Aeronautics and Space Administration.

REFERENCES

BISPO, P.C.; VALERIANO, M.M.; SANTOS, J.R. Effects of the geomorphometric characteristics of local terrain on floristic composition in the central Brazilian Amazon. **Austral Ecology**, v. 37, n. 4, p. 491, 2012.

BLAIR, J. B.; HOFTON, M.A.; RABINE, D.L. Processing of NASA LVIS elevation and canopy (LGE, LCE and LGW) data products, ver- sion 1.01, report, NASA Goddard Space Flight Cent., Greenbelt, Md. (Available at http://lvis.gsfc.nasa.gov), 2006.

CHAVE, J.; CONDIT, R.; AGUILAR, S.; HERNANDEZ, A.; LAO, S.; PEREZ, R. Error propagation and scaling for tropical forest biomass estimates. **Philosophical. Transactions.of Royal Society. B**, v. 359, p. 409, 2004.

CHAVE J.; ANDALO, C.; BROWN, S.; CARINS, M.A.; CHAMBERS, J.Q.; EAMUS, D.; FÖLSTER, H.; FROMARD, F.; HIGUCHI, N.; KIRA, T.; LESCURE, J.P.; NELSON, B.W.;. OGAWA, H.; PUIG, H.; RIÉRA, B.; YAMAKURA, T. Tree allometry and improved estimation of carbon stocks and balance in tropical forests. **Oecologia**, v. 145, p. 87, 2005.

DRAKE, J. B.; DUBAYAH, R.O.; CLARK, D.B.; KNOX, R.G.; BLAIR, J.B.; HOFTON, M.A.; CHAZDON, R.L.; WEISHAMPEL, J.F.; PRINCE, S.D. Estimation of tropical forest structural characteristics using large-footprint LiDAR. **Remote Sensing of Environment**., v. 79, p. 305, 2002.

ECKERT, S. Improved forest biomass and carbon estimations using texture measures from WorldView-

2 satellita data. **Remote Sensing**, v. 4, p. 810, 2012.

HAJNSEK, I.; KUGLER, F.; LEE, S-K.; PAPATHANASSIOU, K.P. Tropical-Forest-Parameter Estimation by Means of Pol-InSAR: The INDREX-II Campaign. **IEEE Transactions on Geoscience. and Remote Sensing**., v. 47, n. 2, p. 481, 2009.

JACKSON, J.D., **Classical Electrodynamics**, John Wiley, New York, 1975.

KRIEGER, G.; MOREIRA, A.; FIEDLER, H.; HAJNSEK, I.; WERNER, M.; YOUNIS, M.; ZINK, M. TanDEM-X: A satellite formation for high resolution SAR interferometry. **IEEE Transactions on Geoscience and Remote Sensing,** v. 45, n. 11, p. 3317, 2010.

LEFSKY, M. A.; COHEN, W.B.; PARKER, G.G.; HARDING, D.J. LiDAR remote sensing for ecosystem studies. **BioScience**, v. 52, n. 1, p. 192, 2002.

LEFSKY, M.A. A global forest canopy height map from the Moderate Resolution Imaging Spectroradiometer and the Geoscience Laser Altimeter System. **Geophysical Research Letter**., v. 37, p. L15401, 2010.

MACARTHUR, R. H.; HORN, H.S. Foliage profile by vertical measurements. **Ecology,** v. 50, p.802, 1969.

NEEFF, T.; DUTRA, L.V.; SANTOS, J.R.; FREITAS, C.C.; ARAUJO, L.S. Tropical forest stand table modeling from SAR data. **Forest Ecology and Management**, v. 186, p. 159, 2003.

NEEFF, T., L. V. DUTRA, L.V.; SANTOS, J.R.; FREITAS, C.C.; ARAUJO, L.S. Tropical forest measurement by interferometric height modeling and P-band radar backscatter, **Forest Science**. v. 51, n. 6, p. 585, 2005a.

NEEFF, T.; DUTRA, L.V.; SANTOS, J.R.; FREITAS, C.C.; ARAUJO, L.S. Power spectrum analysis of SAR data for spatial forest characterization in Amazonia. **International Journal of Remote Sensing**, v.26, n.13, p. 2851, 2005b.

NELSON, R. F.; HYDE, P.; JOHNSON, P.; EMESSIENE, B.; IMHOFF, M.L.; CAMPBELL, R.; EDWARDS, W. Investigating RaDAR-LiDAR synergy in a North Carolina pine forest. **Remote Sensing of. Environment**., v. 110, p. 98, 2007.

SCHLESINGER, W. H. Biogeochemistry: An Analysis of Global Change, Academic Press, San Diego, 1991.

STRATTON, J. A.; CHU, L.J. Diffraction Theory of Electromagnetic Waves. **Physical Review**, Vol. 56, p. 99, 1939.

TREUHAFT, R. N.; MADSEN, S.N.; MOGHADDAM, M.; VAN ZYL, J.J. Vegetation characteristics and underlying topography from interferometric radar. **Radio Science**, v. 31, n. 6, p. 1449, 1996.

TREUHAFT, R. N., ASNER, G.P.; LAW, B.E. Structure-based forest biomass from fusion of radar and hyperspectral Observations, **Geophysical Research Letter**., v. 30, n. 9, 2003.

TREUHAFT, R. N.; LAW, B.E.; ASNER, G.P. Forest attributes from radar interferometric structure and its fusion with Optical Remote Sensing. **BioScience**, v. 54, n. 6, p. 561, 2004.

TREUHAFT, R. N.; CHAPMAN, B.D.; SANTOS, J.R.; GONÇALVES, F. G.; DUTRA, L.V.; GRAÇA, P.M.L.A.; DRAKE, J.B. Vegetation profiles in tropical forests from multibaseline interferometric synthetic aperture radar, field, and LiDAR measurements. **Journal of Geophysical. Research**., v. 114, p. D23110, 2009.

TREUHAFT, R. N.; GONÇALVES, F.G.; DRAKE, J.B.; CHAPMAN, B. D.; SANTOS, J. R.; DUTRA, L.V.; GRAÇA, P.M.L.A.; PURCELL, G.H. Biomass estimation in a tropical wet forest using Fourier trnasforms of profiles from LiDAR or interferometric SAR. **Geophysical Research Letter** ., v. 37, p. L23403, 2010.

TREUHAFT, R. N.; LOWE, S.T.; CARDELLACH, E. Formulating a vector wave expression for polarimetric GNSS surface scattering, **Progress in Electromagnetics Research** B, v. 33, p. 257, 2011.

VAN ZYL, J. J.; Chu, A.; Hensley, S.; Lou, Y.; Kim, Y. The AIRSAR/TOPSAR integrated multi-frequency polarimetric and interferometric SAR processor, *Conf. Publ. 449*, Inst. Of Electr. Eng., New York, p. 100, 1997.